Supplementary Information (SI) for Journal of Materials Advances.
This journal is © The Royal Society of Chemistry 2025

Supporting Information

Design of Experiments guided Hydrothermal Synthesis of $CuFeO_2$ Photocathodes for Photoelectrochemical Hydrogen Evolution

Mohamed El Idrissi,[a,b] Jonathan Pöttker-Menke,[a] Ying Kong,[a] Mohammed Abd-Lefdil,[b] Lahoucine Atourki,[b] and Bastian Timo Mei, [a,*]

[a] Laboratory of Industrial Chemistry, Ruhr-University Bochum, Universitätsstraße 150, 44801 Bochum, Germany. E-mail: bastian.mei@rub.de

[b] MANAPSE Lab, Faculty of Science, Mohammed V University in Rabat, avenue Ibn Batouta, P.B. 1014, Rabat, Morocco

Table S1 : Box-Behnken experimental design matrix and corresponding photocurrent density (E) response measured at 0.4 V vs. RHE for all $CuFeO_2$ photocathodes.

Run Order	Hydrothermal Synthesis Temperature (°C)	Hydrothermal Synthesis Time (Hours)	Annealing Temperature (°C)	Annealing Time (Hours)	Current Density (mA/cm²) at 0.4V vs RHE
1	110	1	600	4	-1.6715
2	170	1	600	4	-1.01167
3	110	12	600	4	-1.18633
4	170	12	600	4	-0.5265
5	140	6.5	550	1	-1.04367
6	140	6.5	650	1	-1.26283
7	140	6.5	550	7	-0.93517
8	140	6.5	650	7	-1.15433
9	110	6.5	600	1	-1.48317
10	170	6.5	600	1	-0.82333
11	110	6.5	600	7	-1.37467
12	170	6.5	600	7	-0.71483
13	140	1	550	4	-1.232
14	140	12	550	4	-0.74683
15	140	1	650	4	-1.45117
16	140	12	650	4	-0.966
17	110	6.5	550	4	-1.31933
18	170	6.5	550	4	-0.6595
19	110	6.5	650	4	-1.5385
20	170	6.5	650	4	-0.87867
21	140	1	600	1	-1.39583
22	140	12	600	1	-0.91067
23	140	1	600	7	-1.28733
24	140	12	600	7	-0.80217
25	140	6.5	600	4	-1.099

Table S2: Full Analysis of Variance (ANOVA) table for the fitted quadratic model, showing that all linear terms (A, B, C, D) are highly significant ($p < 0.05$), while all quadratic and interaction terms are statistically insignificant ($p = 1.000$).

	DF	Sum of Squares	Mean Square	F Value	Prob>F
A	1	1.30614	1.30614	6.5307E10	2.07158E-50
B	1	0.70616	0.70616	3.5308E10	4.48471E-49
C	1	0.1441	0.1441	7.2051E9	1.26736E-45
D	1	0.03532	0.03532	1.76584E9	1.43333E-42
A*A	1	1.30626E-31	1.30626E-31	6.5313E-21	1
B*B	1	1.66213E-31	1.66213E-31	8.31065E-21	1
C*C	1	1.3875E-32	1.3875E-32	6.9375E-22	1
D*D	1	2.30273E-33	2.30273E-33	1.15136E-22	1
A*B	1	1.11657E-31	1.11657E-31	5.58285E-21	1
A*C	1	3.08149E-33	3.08149E-33	1.54074E-22	1
A*D	1	0	0	0	1
B*C	1	3.08157E-33	3.08157E-33	1.54079E-22	1
B*D	1	3.08149E-33	3.08149E-33	1.54074E-22	1
C*D	1	3.10267E-32	3.10267E-32	1.55133E-21	1
Error	10	2E-10	2E-11		
Lack of fit	10	2E-10	2E-11	--	--
Pure Error	0	0	--		
Total	24	2.19172			

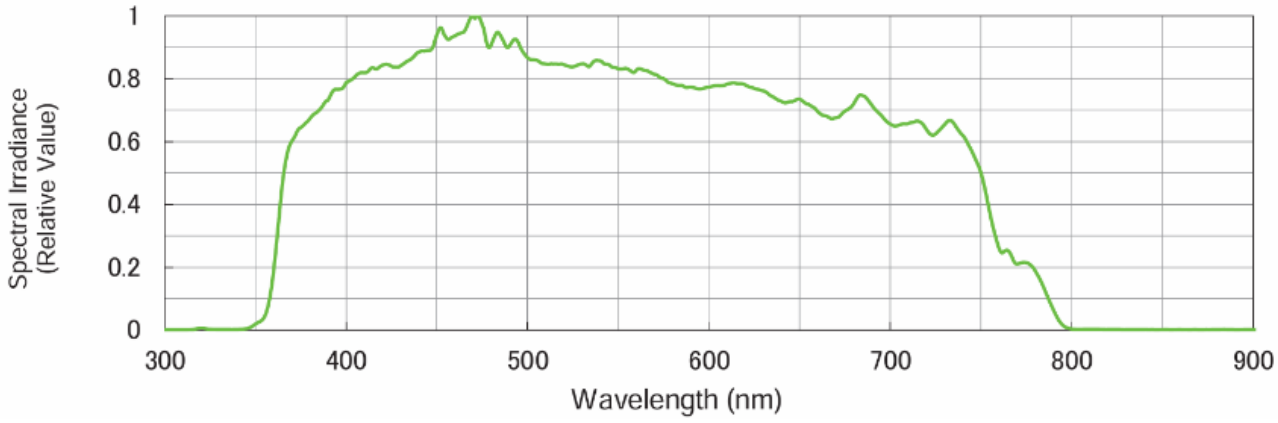

Figure S1: Spectral distribution of MAX-303 with UV Lamp and VIS Mirror Module measured by fiber spectrometer.

To gain further insight into the crystallographic structure, HRTEM analysis was performed on the powder synthesized at 140 °C. Lattice fringe imaging revealed two dominant facet orientations. Figure S2a shows well-defined fringes with a measured spacing of 0.251 nm, corresponding to the (012) plane. The statistical distribution of this spacing, confirmed by histogram analysis (Figure S2b), affirms its prevalence. Similarly, Figure S2c displays lattice fringes with a spacing of 0.152 nm, attributed to the (110) plane, a finding supported by the accompanying histogram (Figure S2d). These results corroborate the XRD findings and confirm that the $CuFeO_2$ crystals predominantly expose (012) and (110) facets.

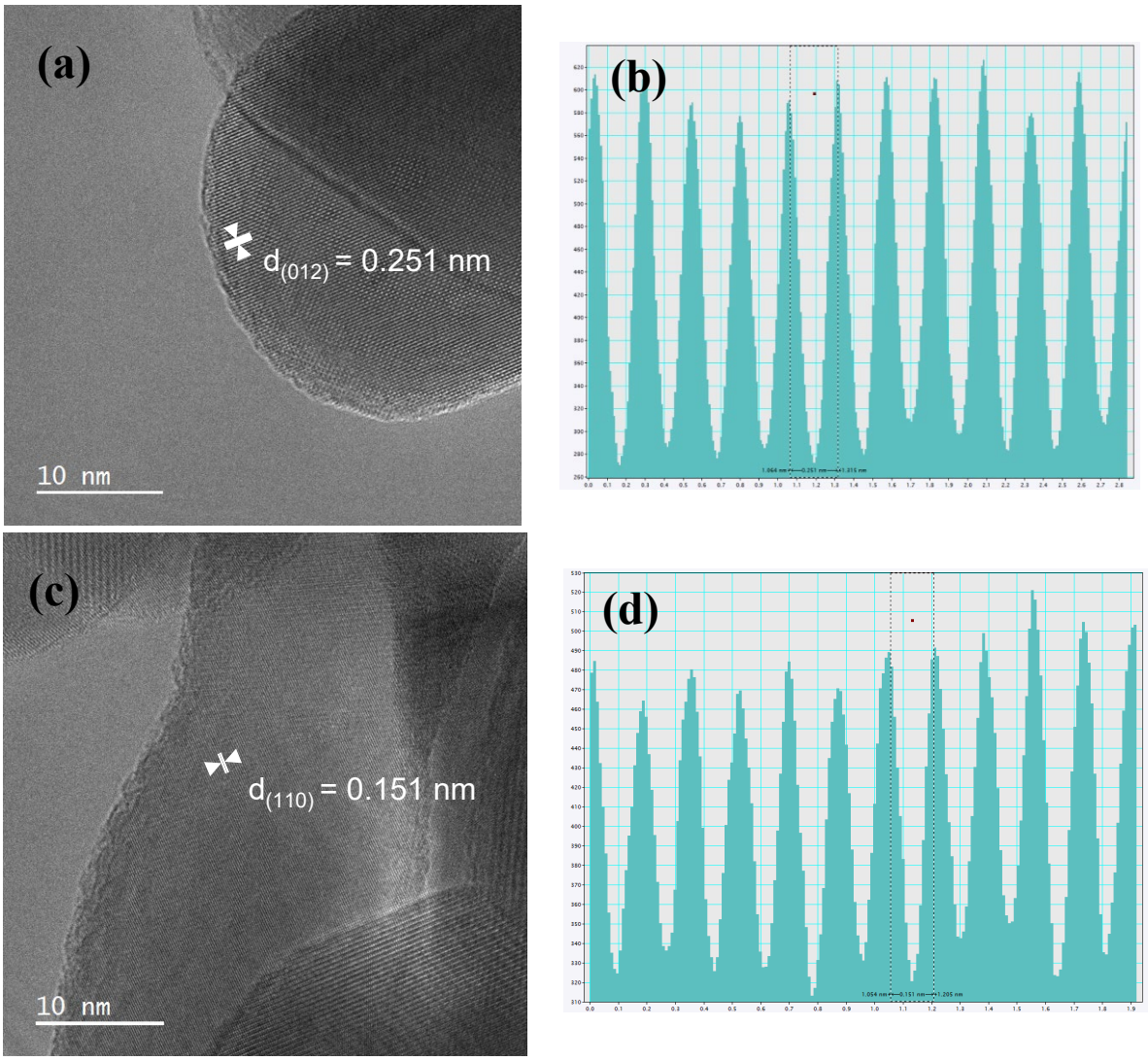

Figure S2: HRTEM analysis of $CuFeO_2$ synthesized at 140 °C for 1 hour confirming dominant facet orientations. (a) Lattice fringes of the (012) plane (d-spacing = 0.251 nm). (b) Histogram of lattice periodicity for the (012) plane. (c) Lattice fringes of the (110) plane (d-spacing = 0.152 nm). (d) Histogram of lattice periodicity for the (110) plane.

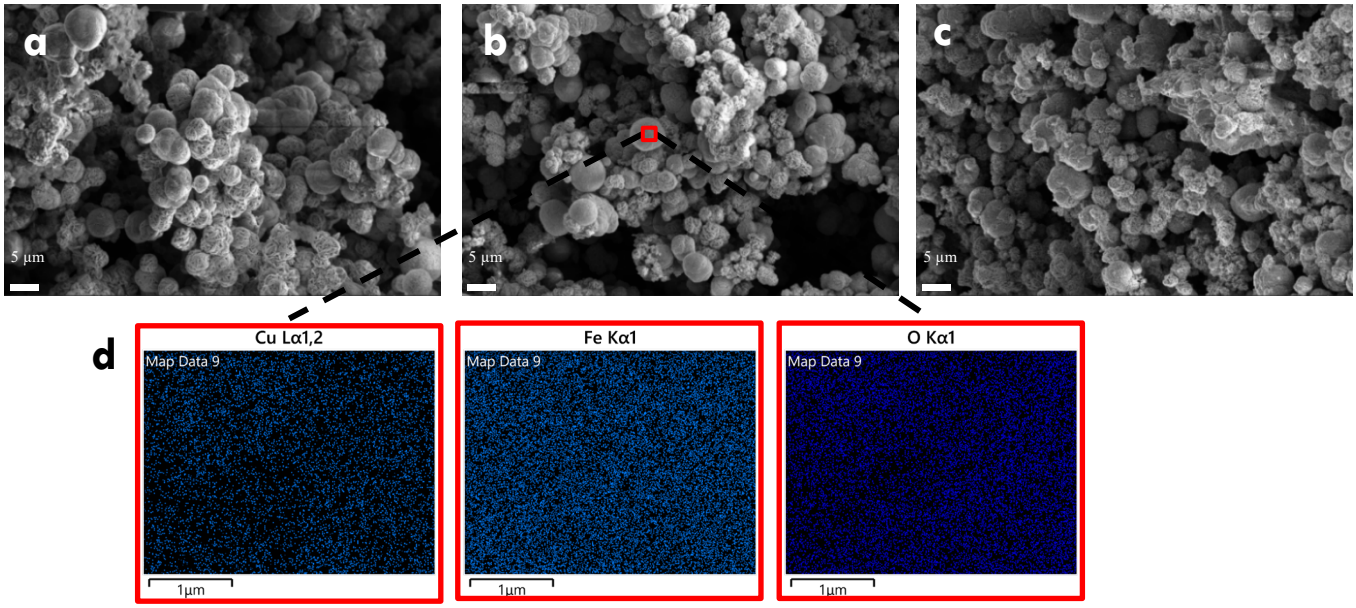

Figure S3: SEM images showing the surface morphology of $CuFeO_2$ powders synthesized at (a) 110 °C, (b) 140 °C, and (c) 170 °C for 1 hour. (d) Elemental mapping (Cu, Fe, O) of the powder synthesized at 140 °C, demonstrating uniform elemental distribution.

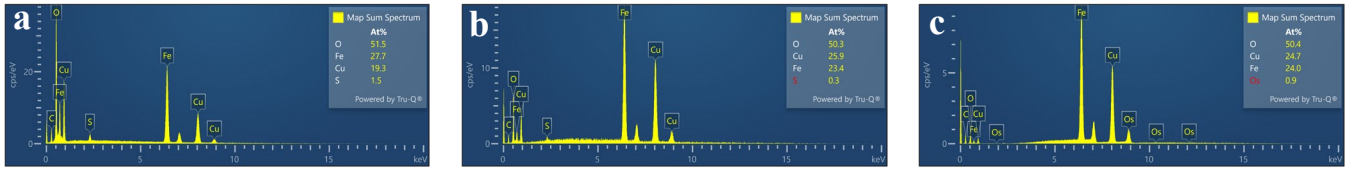

Figure S4: EDX spectra and quantitative atomic percentage analysis (inset) of $CuFeO_2$ powders synthesized at (a) 110 °C, (b) 140 °C, and (c) 170 °C for 1 hour, confirming stoichiometric composition (~50% O, ~25% Cu, ~25% Fe) across all samples.

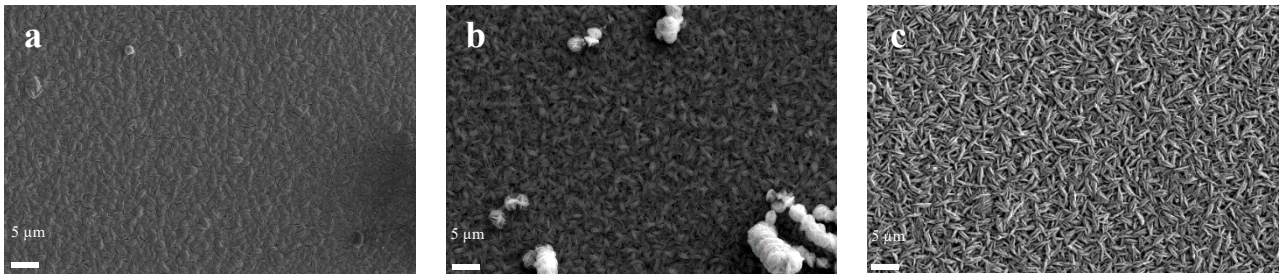

Figure S5: SEM images of as-prepared $CuFeO_2$ thin films derived from powders synthesized at (a) 110 °C, (b) 140 °C, and (c) 170 °C. Films from higher temperature syntheses show denser packing and improved continuity.

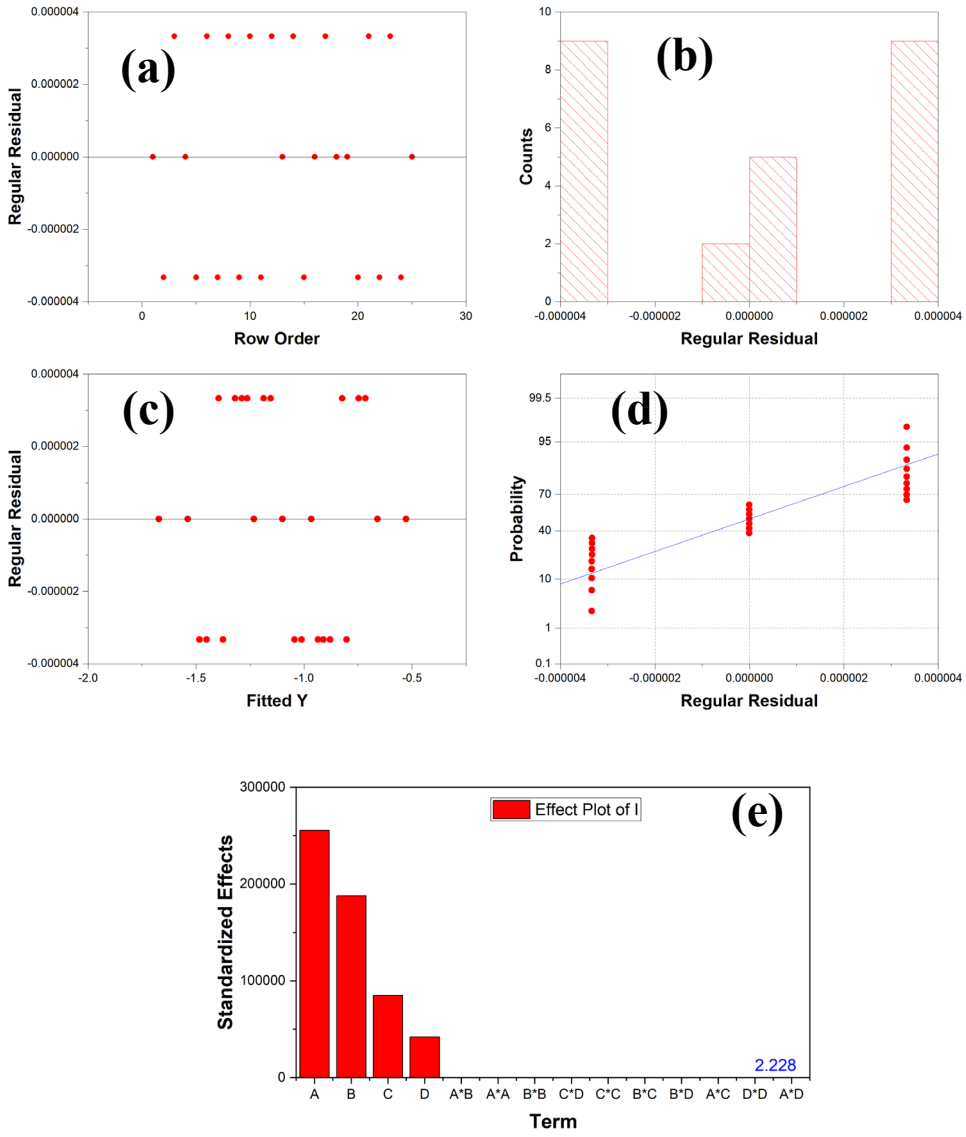

Figure S6: Diagnostic plots for the linear regression model. (a) Residuals versus run order. (b) Histogram of residuals. (c) Residuals versus fitted values. (d) Normal probability plot of residuals. (e) Pareto chart of the standardized effects of the model terms (A: Hydrothermal Temp., B: Hydrothermal Time, C: Annealing Temp., D: Annealing Time).

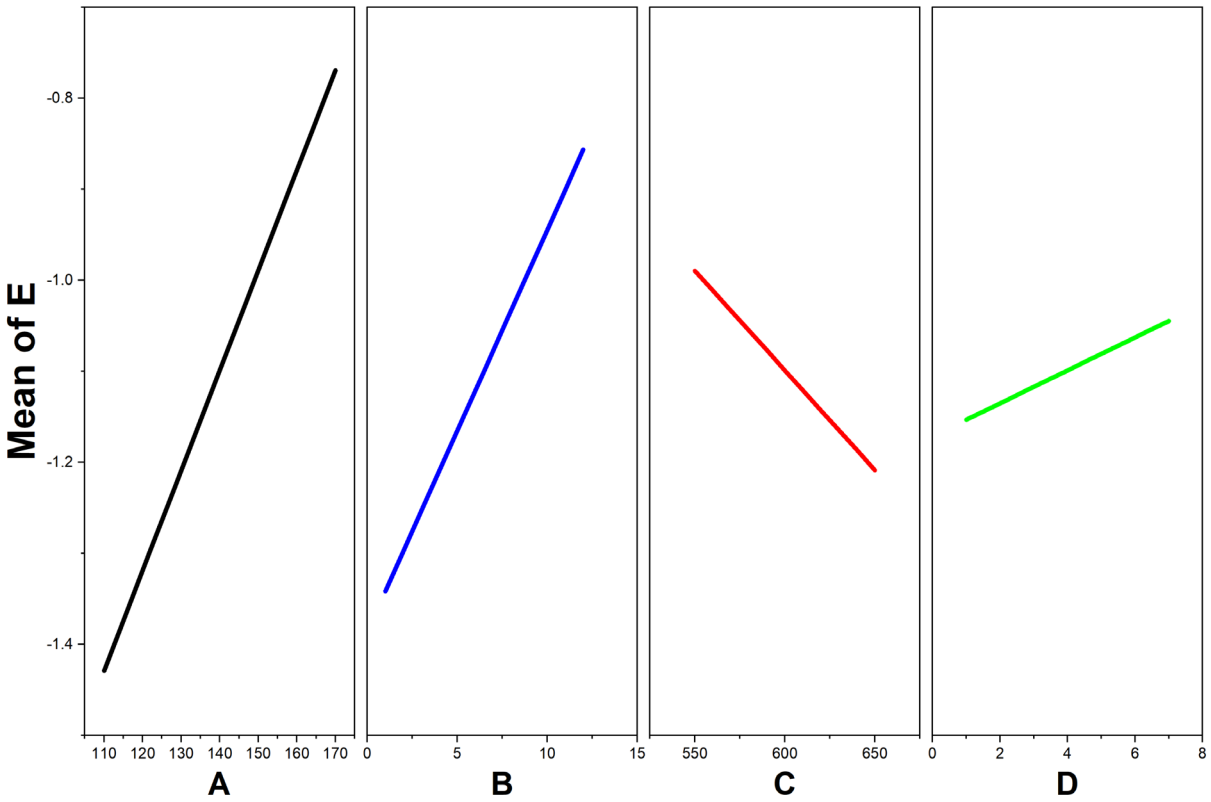

Figure S7: Main effects plots for the four synthesis parameters on photocurrent density at 0.4 V vs. RHE. Hydrothermal temperature (A) is the most influential parameter, with performance decreasing as temperature increases.

Raman Spectrometry

Raman spectroscopy was used to confirm the phase purity and vibrational fingerprint of the in-situ grown films. The $CuFeO_2$ thin films (measured on FTO) and hydrothermally synthesized $CuFeO_2$ powder both show the characteristic Eg and A1g modes at ~342 cm^{-1} and ~692 cm^{-1}, respectively, consistent with the 3R-$CuFeO_2$ structure. The A1g band at ~692 cm^{-1} is assigned to Cu–O stretching vibrations along the c-axis, while the Eg band at ~342 cm^{-1} corresponds to vibrations within the ab-plane. The FTO substrate spectrum is included to show substrate features and to verify that the observed $CuFeO_2$ peaks are not artefacts of the substrate.

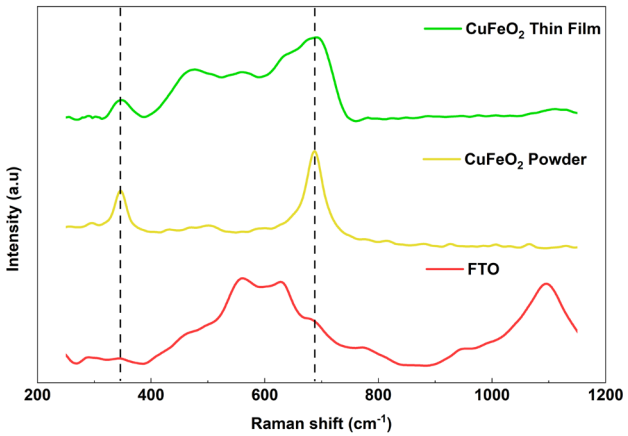

Figure S8: Figure S8. Raman spectra of FTO substrate (red), $CuFeO_2$ powder (yellow), and $CuFeO_2$ thin film on FTO (green). Vertical dashed lines mark the Eg (~342 cm^{-1}) and A1g (~692 cm^{-1}) modes characteristic of 3R-$CuFeO_2$. The $CuFeO_2$ powder and thin-film spectra exhibit the same principal vibrational bands, confirming phase identity. The FTO trace is shown to highlight substrate contributions.

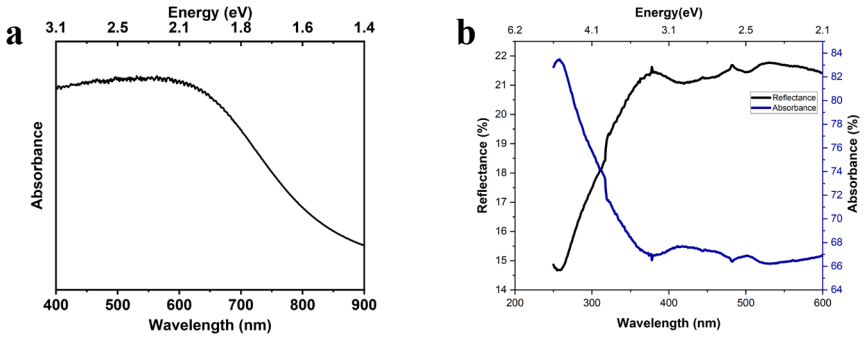

Figure S9: Comprehensive optoelectronic characterization of the optimized $CuFeO_2$ photocathode. (a) UV-Vis absorption spectrum, showing an absorption edge at ~650 nm. (b) Absorbance (T) and reflectance (R) spectra measured with an integrating sphere.

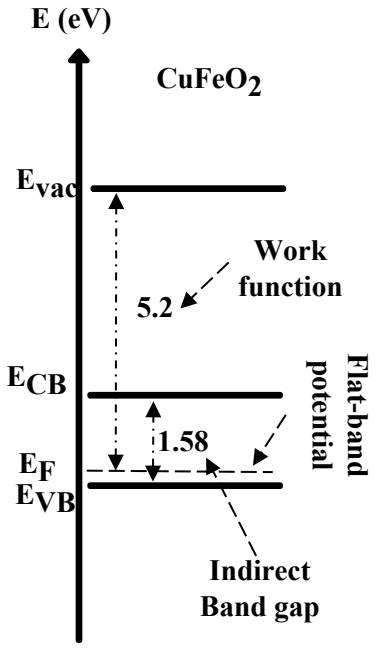

Figure S10: Energy band diagram of $CuFeO_2$ constructed from experimental data, showing favourable band alignment for hydrogen evolution. The photocathode was synthesized hydrothermally at 110 °C for 1 h and annealed at 650 °C for 1 h.

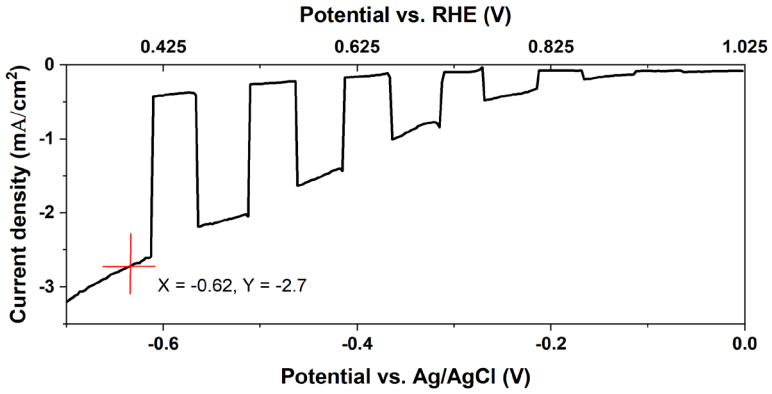

Figure S11: Oxygen reduction reaction (ORR) activity. LSV of the optimized $CuFeO_2$ photocathode measured in O_2-saturated 1 M NaOH under 1 Sun illumination, showing a photocurrent density of −2.7 mA cm^{-2}.

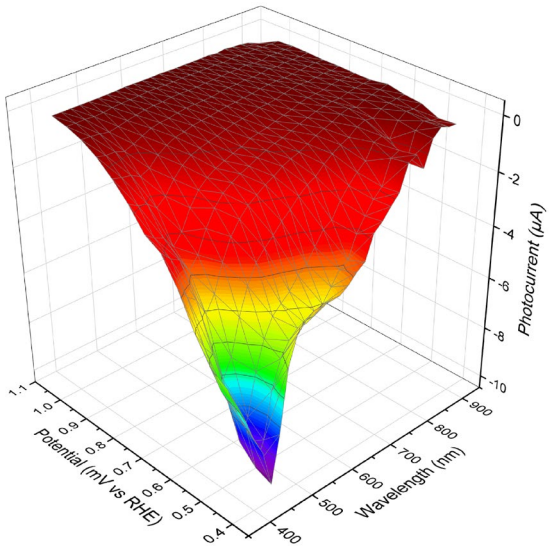

Figure S12: Wavelength-Dependent Photocurrent Response of Optimized $CuFeO_2$ Photocathode on FTO in in N_2-Saturated 1 M NaOH.

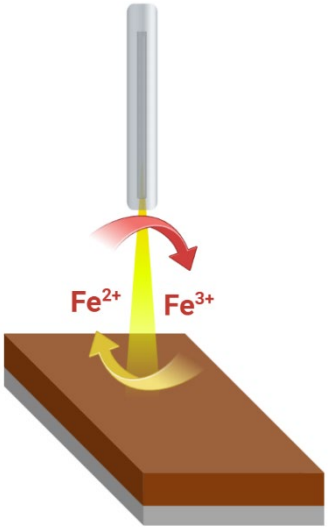

Figure S13: Schematic of the SPECM measurement: optical coupling to the Au microelectrode tip and the electrochemical configuration (Au tip at +1.5 V vs RHE, CuFeO2 at +0.4 V vs RHE).

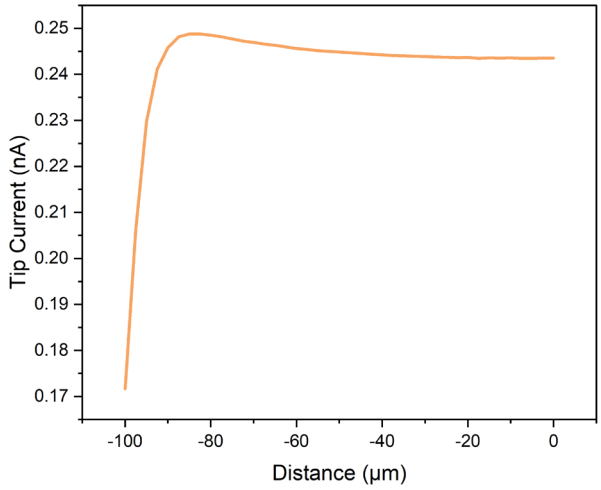

Figure S14: Z-approach curves for SPECM tip positioning. Negative feedback approach curves recorded in 5 mM potassium ferricyanide and 100 mM KCl with the tip polarized at 0.5 V vs. Ag/AgCl and the $CuFeO_2$ electrode unbiased.

Calculation of Solar Photocurrent Density from IPCE Data

To estimate the theoretical solar photocurrent density of the optimized $CuFeO_2$ photocathode, we numerically integrated the wavelength-dependent incident photon-to-current efficiency (IPCE) with the corresponding incident light power. The calculation was performed using Python, based on the following equation:

$$J_{ph}=q\int IPCE(\lambda)\times\Phi(\lambda)d\lambda \quad (1)$$

Where:

- J_{ph} is the solar photocurrent density (A/cm²)
- q is the elementary charge (1.602×10^{-19} C)
- $PCE(\lambda)$ is the IPCE at wavelength λ\lambda (unitless)
- $\Phi(\lambda)$ is the photon flux (photons/cm²·s·nm), calculated from the incident light power

The photon flux at each wavelength was computed using:

$$\Phi(\lambda)=\frac{P(\lambda)}{hc/\lambda} \quad (2)$$

Where:

- $P(\lambda)$ is the incident light power in watts (converted from μW)
- h is Planck's constant (6.626×10^{-34} J·s)
- c is the speed of light (3×10^{8} m/s)
- λ is the wavelength in meters

The IPCE data were stored in an Excel file named IPCE.xlsx, containing three columns: Wavelength (nm), IPCE (%) and Incident light (μW), The IPCE values were converted to fractional form, and the incident light power was used to calculate the photon flux at each wavelength. The integration was performed using the trapezoidal rule, and the final result was converted to mA/cm² for comparison with experimental PEC measurements.

Energy-metric calculations

The calculations below use the experimentally measured H_2 production rate Figure S16 and Faradaic efficiency: H_2 rate = 1.036 μmol·h^{-1}, FE ≈ 0.40, Chronoamperometry (CA) duration t=1 h=3600 s, illuminated area A=1.0 cm^2, and the working electrode potential V_{WE}= 0.5 V vs RHE. The Faraday constant is F=96485 C mol^{-1} and the Gibbs free energy for H_2 formation is $\Delta G^{\circ}\approx237$ kJmol^{-1}.

Moles of H_2 produced during the 1 h CA (from GC):

$$n_{H_2}=1.036\ \mu mol\ (over\ 1h). \quad (3)$$

Total charge that would be required to produce this H_2 at 100% FE:

$$Q_{theor} = 2Fn_{H_2} = 2 \times 96485 \times 1.036\ 10^{-6} = 0.2\ C \quad (4)$$

Total measured charge consistent with the FE: Because FE = (H_2 produced) / (H_2 expected from charge), the measured total charge Q_{meas} is:

$$Q_{meas} = \frac{Q_{theor}}{FE} = \frac{0.2}{0.4} = 0.49\ C. \quad (5)$$

Average current during the CA (over 1 h):

$$I_{avg} = \frac{Q_{theor}}{FE} = \frac{0.49}{3600} = 139\ \mu A \quad (6)$$

Electrical energy input (working-electrode basis) during the 1 h CA:

$$E_{elec} = V_{WE} \times Q_{meas} = 0.25\ J. \quad (7)$$

Electrical energy per mole of H_2 (corrected for FE):

$$E_{per\ mol} = \frac{E_{elec}}{n_{H_2}} = 241\ KJ\ mol^{-1} \quad (8)$$

$$E_{per\ Kg} = 33.2\ KWh\ Kg^{-1} \quad (9)$$

Solar-to-hydrogen (STH) efficiency estimate (illumination basis):

The H_2 production rate is: $\dot{n}_{H_2} = n_{H_2}/t = 1.036/3600 = 2.878\ 10^{-10} mol\ s^{-1}$. The chemical power stored as H_2 is:

$$P_{chem} = \dot{n}_{H_2} \times \Delta G^0 = 6.82\ 10^{-6}\ W \quad (10)$$

With incident optical power Pin = 100 mW, the STH efficiency is:

$$\eta_{STH} = \frac{P_{chem}}{P_{in}} = 0.068\ \% \quad (11)$$

Using the GC-measured H_2 rate (1.036 µmol·h^{-1}) and the Faradaic efficiency (≈40%), the working-electrode energy input (at +0.5 V vs RHE) corresponds to an electrical energy consumption of ≈241 kJ·mol^{-1} H_2 (≈33.2 kWh·kg^{-1}). The estimated STH efficiency based on incident 1-sun illumination (100 mW·cm^{-2}, 1 cm²) is ≈0.068 %. These values are reported on a working electrode basis (WE potential × charge) and do not include any additional cell or counter electrode losses.

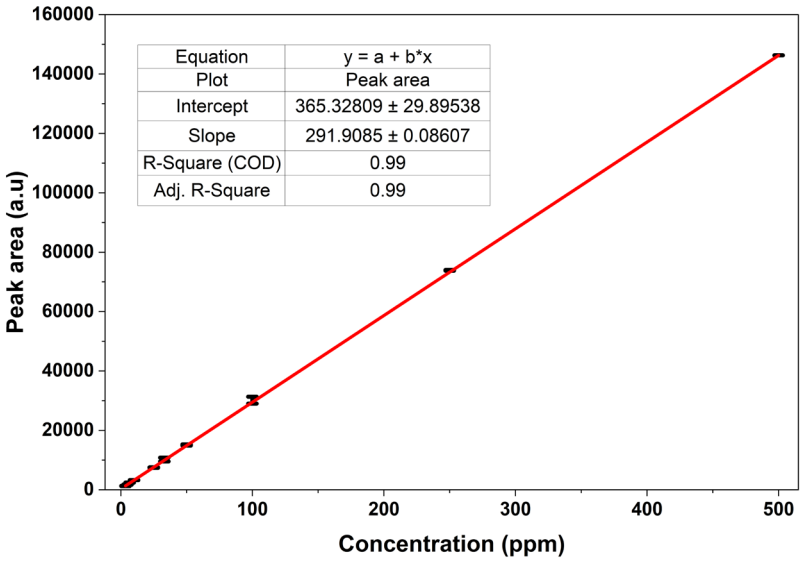

Figure S15: Calibration curve for hydrogen quantification by gas chromatography. The linear fit was performed using peak area (a.u.) versus H_2 concentration (ppm), yielding a slope of 291.9 and R^2 = 0.99. This calibration was used to calculate the H_2 evolution rate and Faradaic efficiency.

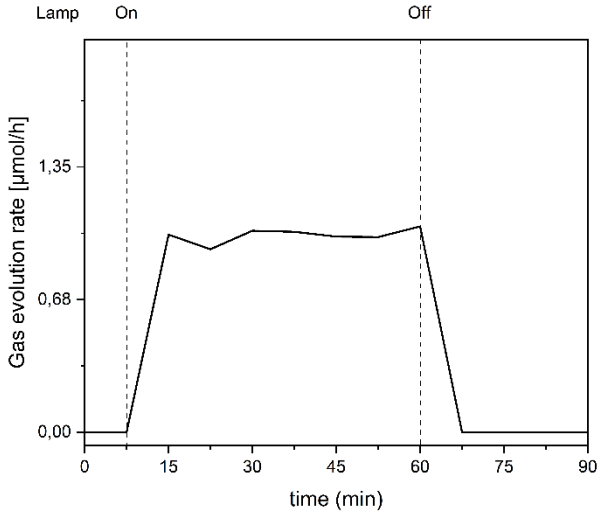

Figure S16: Hydrogen evolution rate vs time measured by online GC-BID during the 1 h CA at +0.5 V vs RHE, light on periods produce a constant H_2 generation rate of 1.036 µmol h^{-1}, which drops to ≈0 when illumination is turned off, integrated H_2 and the corresponding charge yield an average Faradaic efficiency of ≈40%.

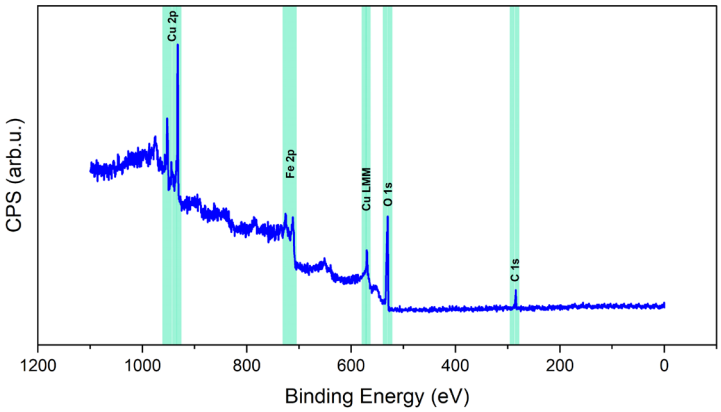

Figure S17: XPS survey spectrum of the pristine $CuFeO_2$ photocathode. The spectrum confirms the presence of Cu, Fe, and O with no detectable impurities.

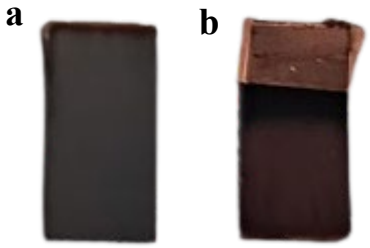

Figure S18: Visual evidence of degradation. Photographic images of the $CuFeO_2$ electrode (a) before and (b) after PEC operation, showing a colour change from dark green to brown.

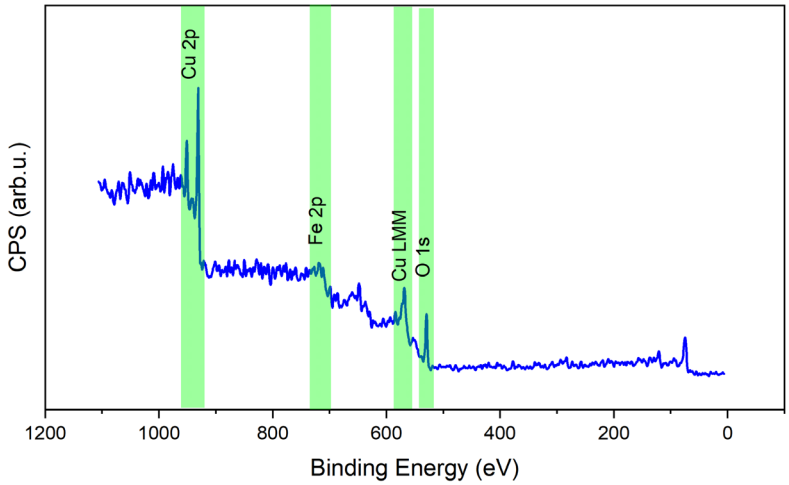

Figure S19 : XPS survey spectrum of $CuFeO_2$ after PEC operation. The spectrum confirms that no external contaminants were introduced during PEC testing, despite the severe chemical reduction of the film.

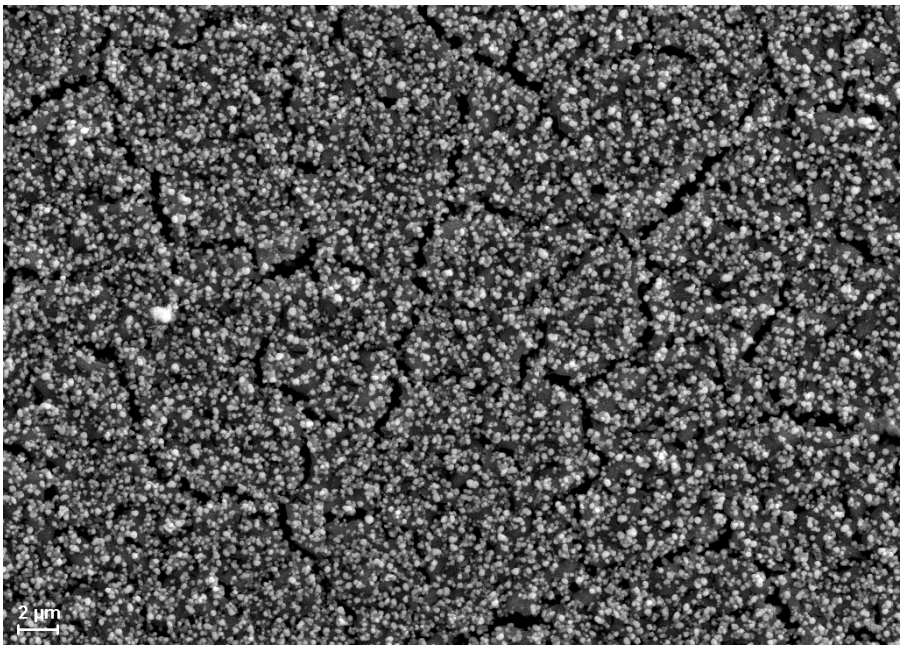

Figure S20: SEM image of $CuFeO_2$ after PEC operation. The micrograph shows significant morphological degradation, including agglomeration, consistent with the chemical instability revealed by XPS.

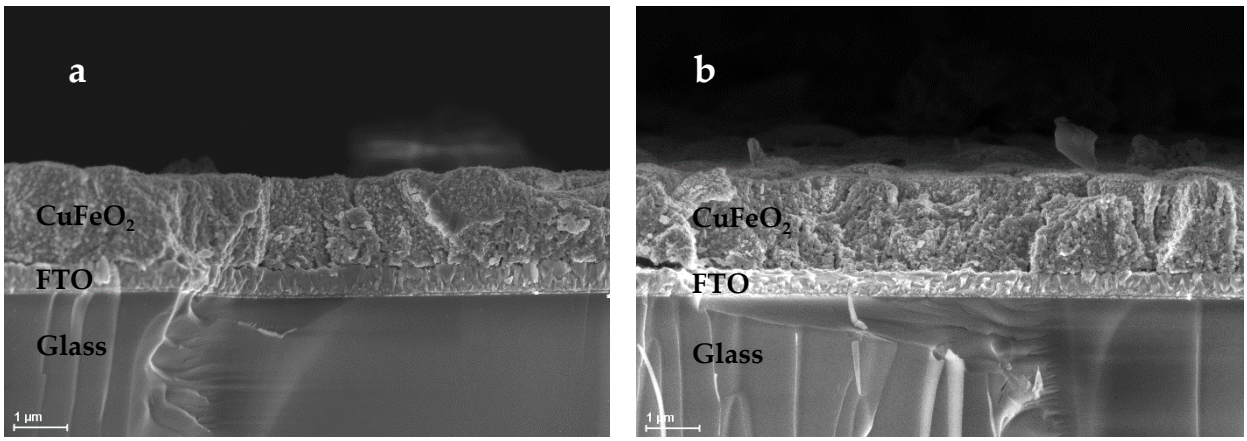

Figure S21: Cross-sectional SEM of FTO/$CuFeO_2$ photocathode (a) before PEC testing and (b) after 1-h chronoamperometry at +0.5 V vs RHE under 1-sun illumination.

Table S3: Comparative semiconductor and EIS parameters for bare $CuFeO_2$ photocathodes.

Study	Indirect band gap (eV)	Direct band gap (eV)	Flat-band potential (V vs RHE)	R_s ($\Omega \cdot cm^2$)	R_{ct} (dark) ($\Omega \cdot cm^2$)	R_{ct} (light) ($\Omega \cdot cm^2$)	C_{sc} (dark) ($\mu F \cdot cm^{-2}$)	C_{sc} (light) ($\mu F \cdot cm^{-2}$)
This work	1.58	3.01	+1.01	17	104	89.2	7.7	15
Prévot et al.,	1.47	3.10	+1.01	-	-	-	-	-
Präg et al.,	1.44 (Tauc) , 1.17 (phonon-corrected)	3.30	+1.10	-	-	-	-	-

Table S4: Photoelectrochemical performance parameters for bare $CuFeO_2$ photocathodes

Study	Photocurrent for ORR (O_2, +0.4 V vs RHE)	Photocurrent for HER (N_2/Ar, +0.4 V vs RHE)	IPCE / APCE (wavelength, potential)	H_2 evolution rate ($\mu mol \cdot h^{-1}$)	Faradaic Efficiency (FE)
This work	2.7 $mA \cdot cm^{-2}$	1.7 $mA \cdot cm^{-2}$	IPCE 16% (400 nm, +0.4 V vs RHE), APCE 20% at 400 nm (+0.4 V vs RHE)	0.0076 $\mu mol \cdot h^{-1}$	≈ 40% (1 h CA at +0.5 V vs RHE, N_2, 1 M NaOH)
Prévot et al.[1]	1.05 $mA \cdot cm^{-2}$	negligible/poorly quantified	IPCE >10% at 400 nm (measured at +0.4 V vs RHE)	-	-
Präg et al.[2]	0.3 $mA \cdot cm^{-2}$	very low ($\mu A \cdot cm^{-2}$ range)	IPCE up to ≈12.5% at 400 nm (measured at +0.4 V vs RHE)	-	-

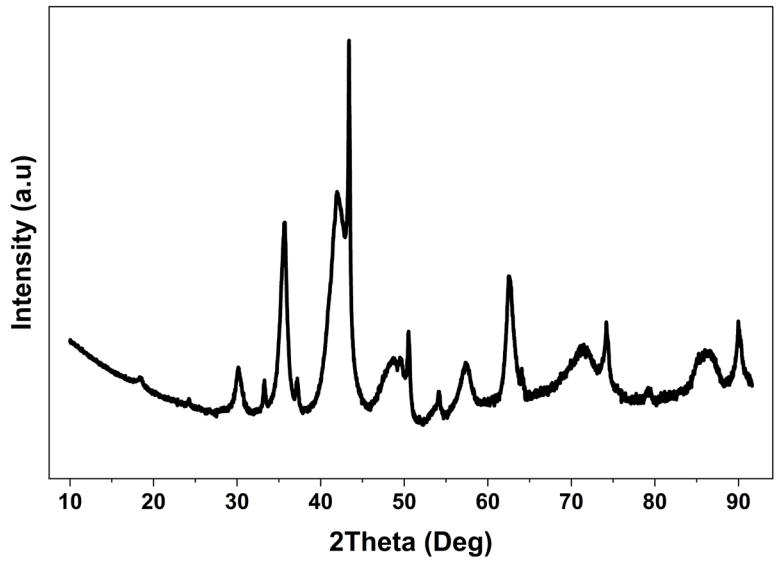

Figure S22: Post-catalysis X-ray diffraction (XRD) pattern of the $CuFeO_2$ photocathode after after 1-h chronoamperometry at +0.5 V vs RHE under 1-sun illumination. Note that the pattern was obtained from the powder scratched off the electrode.

References

1. Prévot, Mathieu S., Néstor Guijarro, and Kevin Sivula. "Enhancing the performance of a robust sol–gel-processed p-type delafossite $CuFeO_2$ photocathode for solar water reduction." *ChemSusChem* 8.8 (2015): 1359-1367.
2. Präg, Raphael, et al. "Photoelectrochemical Properties of $CuFeO_2$ Photocathodes Prepared by Pulsed Laser Deposition." *Chemistry of Materials* 36.16 (2024): 7764-778